Int J Adv Manuf Technol (2018) 94:827–834
DOI 10.1007/s00170-017-0903-z

ORIGINAL ARTICLE

Characterization of heat-treated gas metal arc-welded boron steel sheets

K. I. Yaakob[1] · M. Ishak[1] · S. R. A. Idris[1] · M. H. Aiman[1] · M. M. Quazi[1]

Received: 17 April 2017 / Accepted: 31 July 2017 / Published online: 19 August 2017

Abstract The effect of heat treatment on the microstructure and mechanical properties of 1.6-mm-thick boron steel welded by using gas metal arc welding was investigated. The microstructure and mechanical properties of welded boron steel were determined before and after heat treatment. The heat treatment process was conducted according to manufacturer recommendation for optimum outcome. In results, the microstructure of heat treated specimen was completely transformed to martensite. The soften region that was detected and caused fracture of tensile test is located. EDX analysis found that boron element was concentrated at heat-affected zone. Fractography on heat-treated samples shows an intergranular fracture at heat-affected zone because of microvoid existence at grain boundaries. Consequently, this fracture decreased sample strength and promoted fracture propagation.

Keywords Boron steel (22MnB5) · Boron steel welding · Fusion welding · GMAW

1 Introduction

Advanced high strength steel (AHSS) is a promising metal satisfying the desired requirement in safety, fuel efficiency, emissions, manufacturability, durability, and quality at a low cost. This metal could replace high-strength steel (HSS) materials in automotive industry [1, 2]. Thin components or parts can be designed, and the same load-bearing capability and balanced crash test performance can be maintained using AHSS instead of HSS [3–7].

Boron steel is an AHSS material commonly utilized in the automotive industry. Heating to austenitic temperatures (850–950 °C) and rapid cooling through quenching process transforms boron steel properties from HSS to AHSS. These properties offer more than 1500 MPa of ultimate tensile strength (UTS) value after heat treatment with reasonable material and processing costs. Tensile strength is enhanced by the existence of boron alloying element; consequently, the microstructure is changed, and hardenability is increased [8–12]. Boron will increase the steel hardenability by retarding the heterogeneous nucleation of ferrite at the austenite grain surfaces during rapid cooling. The reduction in interfacial energy, as the boron segregates to the grain boundaries and suppresses the ferrite segregation, resulted in increasing the volume fraction of bainite and martensite as the boron content increases.

Complete austenitization during heating process is a must. An incomplete austenitization condition during heating leads to the inhomogeneous carbon distribution and will cause the lower strength result [13]. Then, the cooling condition is referring to continuous cooling transformation (CCT) diagram prepared by Naderi in 2007 as shown in Fig.1 [14]. According to the diagram, 25 °C/s is the optimum value of cooling rate to transform the austenite to martensite. Otherwise, the slower cooling rate will reduce the volume fraction of martensite and reduce its hardenability. On the other hand, the high austenitizing temperature during heating process can increase the boron segregation at austenite grain boundaries. This segregation might trigger the formation of borocarbide, $M_{23}(C,B)_6$, which can act as a nucleation site for ferrite [15]. Thus, the excessive amount of boron at austenite grain boundaries not only lowers the hardenability, but it also could decrease its toughness, cause embrittlement and produce hot shortness [9, 16]. It commonly happens in fusion welding

✉ M. Ishak
mahadzir@ump.edu.my

[1] Faculty of Mechanical Engineering, Universiti Malaysia Pahang, 26600 Pekan, Pahang, Malaysia

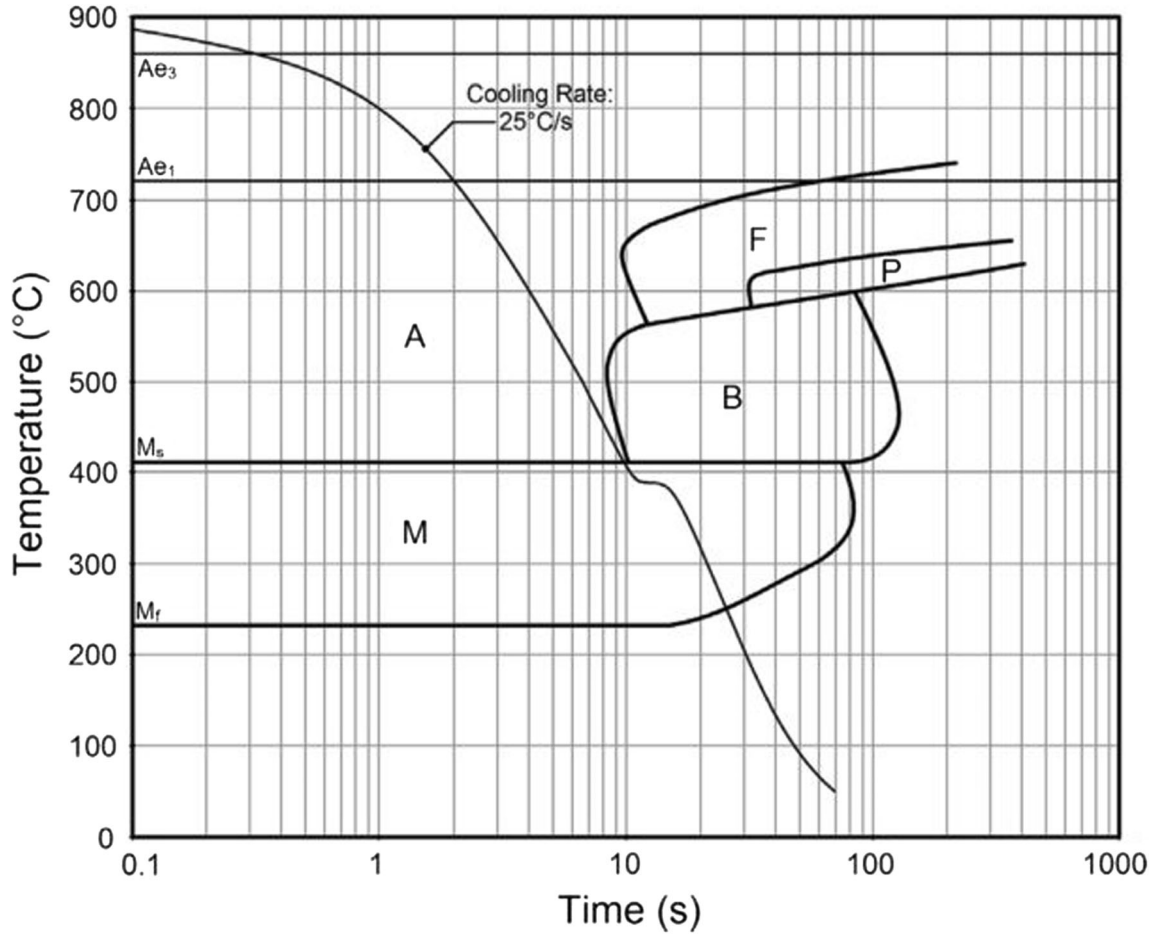

Fig. 1 Continuous cooling transformation (CCT) diagram of 22MnB5 [14]

process which the peak temperature applied to the welded zone could increase the chances of borocarbide precipitation at the heat-affected zone (HAZ).

The application of boron steel in vehicle chassis components is related with welding during assembly stages. Welding process plays a major role in maintains and improves quality, performance, and productivity [13–15]. Additionally, the heat experienced on boron steel during fusion welding increases the challenge and attracts considerable research attention for its behavior. Few research studies regarding the welding of the martensitic phase of boron steel were performed by using several types of welding. In 2009, Bonnen [17] used gas metal arc welding (GMAW) on AHSS body sheet with a combination of dissimilar materials. He focused on the fatigue properties of welded joint. Suh [18] also used GMAW with ER70S-G welding filler in simulating the chassis assembly for quenched boron steel and FB590. He mentioned that increased heat input at welding area reduces hardness, which is known as a softening effect. This effect exists at HAZ located near the fusion zone (FZ) and results in fatigue crack propagation. Similarly, Jong [19] also simulated chassis assembly. He used resistance spot welding on heat treated boron steel and also found the softening effect at the welded area. According to him, the temperature distribution over Ac_3 (temperature needed for complete transformation of ferrite to austenite) during welding will reproduce the martensite microstructure after rapid cooling at ambient air. However, the area that experienced Ac_1 (austenite begins to form) temperature shows a martensite microstructure transformed to a tempered martensite. The softening behavior exists at the

Table 1 Chemical composition of boron steel and ER 70S-6 welding filler

Composition %	C	Si	Mn	P	S	Cr	Ni	B
Boron steel	0.25	0.32	1.23	0.014	0.003	0.17	0.038	0.003
ER70S-6	0.06–0.15	0.80–1.15	1.40–1.85	0.025	0.035	0.15	0.15	–

Table 2 Experimental setup

Working parameters	Description
Welding process	DCEP-Pulse GMAW
Shielding gas	25 L/min-CO_2
Arc length	10 mm
Workpiece material	Boron steel (22MnB5)
Size of workpiece	100 mm × 75 mm
Filler metal	ER70S-6 (1.2 mm diam.)
Current	74.7 Å
Voltage	19.73 V
Weld speed	5 mm/s
Heat input	0.295 kJ/mm

tempered zone. Furthermore, Lin and Ying [20] applied gas tungsten arc welding on a high-boron Fe–Ti–B alloy. They obtained good-quality weld with deteriorating properties because of coarsening weld metal microstructure.

The deterioration properties of welded boron steel after heat treatment are broadly discussed. Nevertheless, limited studies about GMAW application on boron steel join before and after heat treatment, specifically on microstructure and mechanical properties. Therefore, the present research investigated the effect of heat treatment on the microstructure and mechanical properties of boron steel welded through GMAW. Mechanical properties are determined by using tensile and hardness tests. The relationship between microstructure and mechanical properties is also discussed.

2 Experimental procedure

Boron steel (22MnB5) with 1.6 mm thickness was used. The specimen with 75 mm × 100 mm (width × length) dimension was prepared for butt joint configuration during welding [21]. A semi-automated GMAW machine (Dr. Well, DM-500EF) and AWS ER70S-6 carbon steel filler were used in this experiment. The ER70S-6 welding filler was chosen due to higher percentage of manganese and silicon element which incorporates the proper deoxidizer and provide better wetting at the weld toe. The chemical compositions of boron steel and welding filler are shown in Table 1. The experimental setup for welding is shown in Table 2. Three samples of tensile tests were extracted from each welded specimen according to ASTM E8-09 (subsize) standard, as shown in Fig. 2. For heat-treated sample, heating temperature was decided to be at 860 °C which in the austenitization temperature region of steel contains 0.2% of carbon according to iron-carbon phase diagram. With 5 min of soaking temperature inside a continuous-feed furnace, it will allow the steel for microstructural homogenization of austenite. Then, the sample was quenched using water medium at room temperature. The water medium will provide cooling rate higher than critical value as stated by Naderi [14].

Tensile tests were conducted on samples with and without heat treatment. Vertical tensile test was set at a crosshead rate of 1 mm/min, and the UTS value was obtained. For microstructure and hardness observations, the cross sections of both samples were mounted, ground, and etched by using 2% Nital solution. Hardness test was performed by using HV 0.5 according to ASTM E384 standards. Microstructure observation was conducted using an optical microscope and a scanning electron microscope (SEM). Electron-dispersive X-ray (EDX) analysis was performed across the welded area for elemental analysis.

3 Result and discussion

3.1 Microstructure analysis

The microstructures of specimens with and without heat treatment, as observed using an optical microscope, are shown in Figs. 3 and 4. SEM results in Figs. 5 and 6 show clear microstructure images of the welded boron steel. According to Fig. 3a, the base metal microstructure consisted of ferrite (F) and pearlite (P). These phases transformed to austenite because of high heat input during the welding process. After welding, needle-shaped martensite (M) is observed at HAZ, as shown in Fig. 3b. It is located near FZ because this area experienced the peak temperature and high cooling rate during welding. According to Suh [18], martensite formation easily occurs because the martensite starting temperature of boron steel is

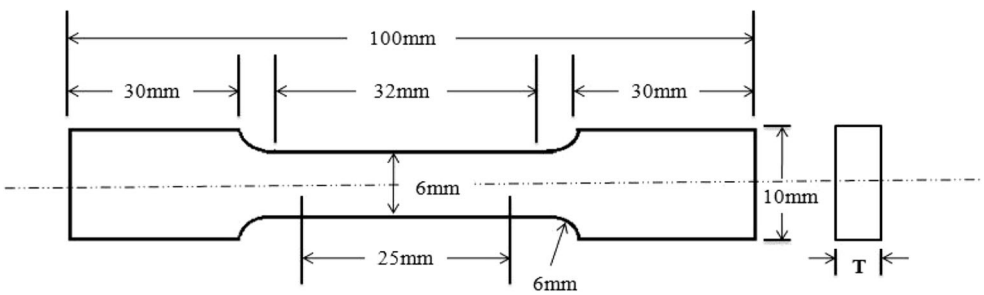

Fig. 2 ASTM E8-09 (subsize) tensile test sample

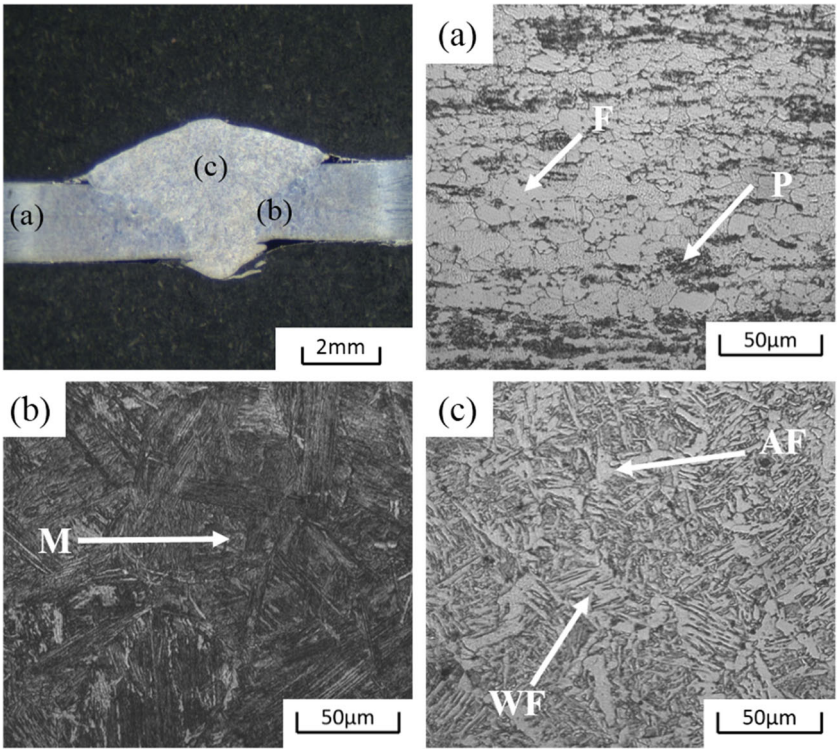

Fig. 3 Microstructure of specimen without heat treatment with × 50 magnification at **a** base metal, **b** HAZ, and **c** FZ consist of ferrite (F), pearlite (P), martensite (M), acicular ferrite (AF), and Widmanstatten ferrite (WF)

low. The temperature and cooling rates during welding are reduced as they moved away from FZ to the base metal. This observation is in agreement with that of Li [22], who found that such condition results in the formation of various phases, including bainite and ferrite, at the area experiencing heat below Ac_1 temperature. Various microstructure types in welded area also depend on welding heat input and cooling rate gradient. Acicular ferrite (AF) and Widmanstatten ferrite (WF) existed in

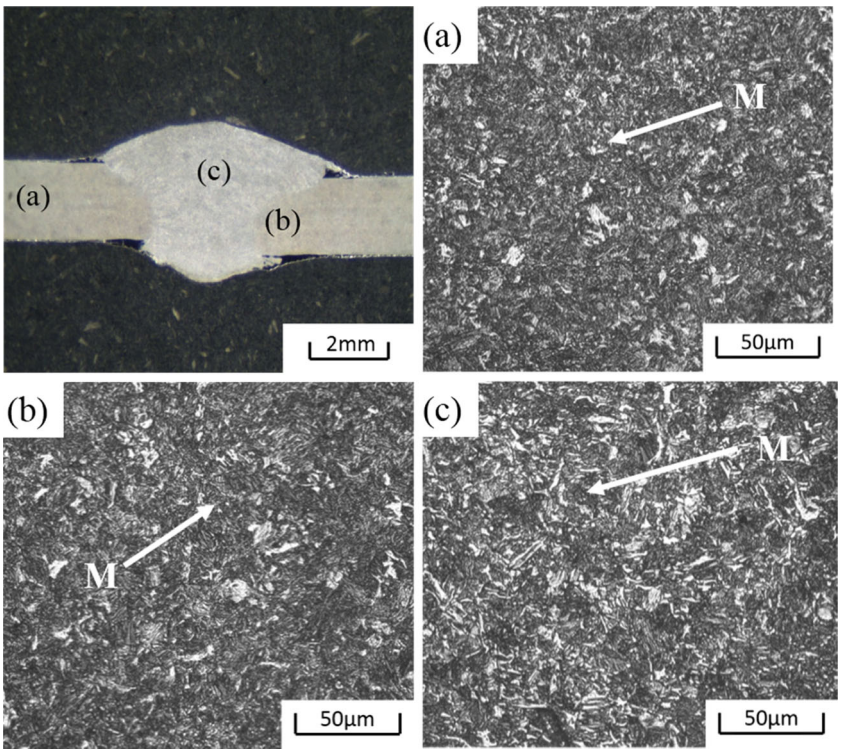

Fig. 4 Microstructure of heat-treated specimen with × 50 magnification at **a** base metal, **b** HAZ, and **c** FZ consist of martensite (M)

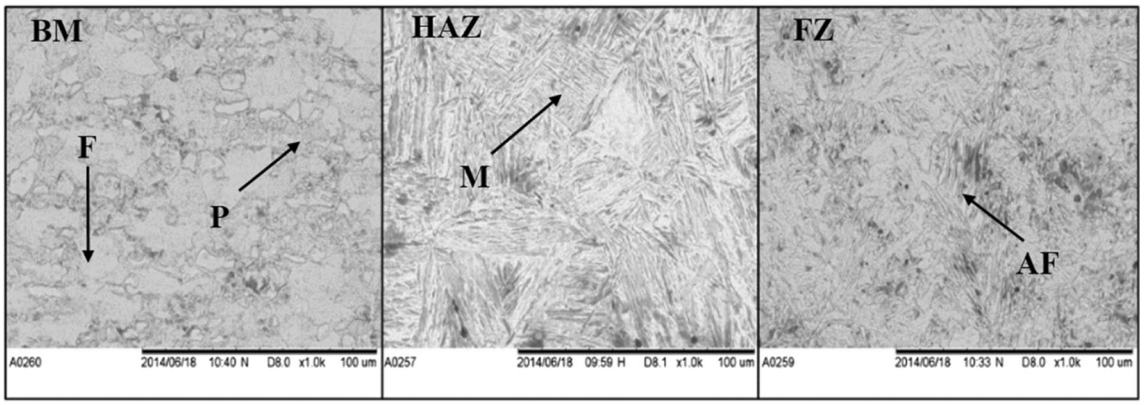

Fig. 5 Microstructure of specimen without heat treatment under SEM with × 1.0 k magnification shows ferrite (F) and pearlite (P) at BM, martensite (M) at HAZ, and acicular ferrite (AF) at FZ

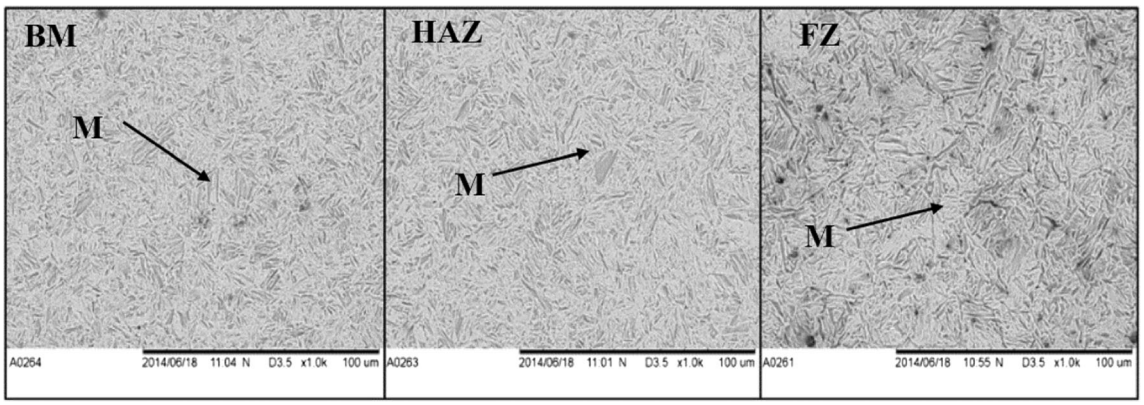

Fig. 6 Microstructure of heat-treated specimen under SEM with × 1.0 k magnification shows martensite (M) at BM, HAZ, and FZ

FZ, as shown in Fig. 3c. In addition to rapid cooling with ambient air at room temperature after welding, the existence of AF might also be due to the non-metallic inclusion added on weld metal, which promotes ferrite nucleation. Moreover, WF nucleation might occur directly from austenite or allotriomorphic ferrite/austenite grain boundaries [23].

The base metal microstructure of heat-treated specimen was completely transformed into martensite, as shown in Figs. 4 and 6. Heat treatment changed the overall microstructure from austenite to martensite. The mechanical properties of different microstructures in the welded area were explained by the hardness test results.

3.2 Hardness test

The hardness behavior of both specimens is shown in Fig. 7. The highest hardness value of the specimen without heat treatment is located at HAZ with 493 HV, followed by FZ and then base metal sequentially as shown in Fig. 7a. The average hardness value at FZ was 284 HV, which was lower than that at

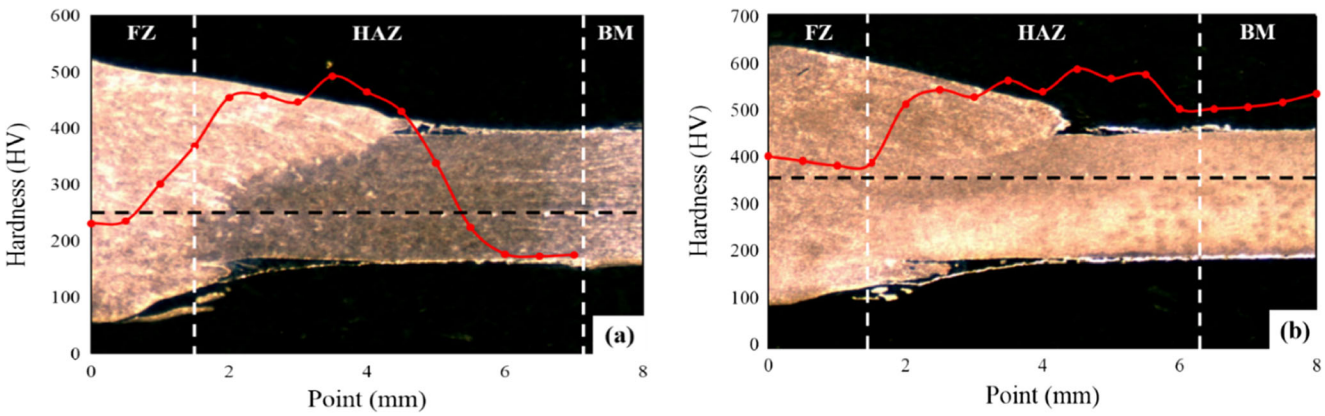

Fig. 7 Macrostructure image and Vickers hardness test for **a** specimen without heat treatment and **b** heat-treated specimen

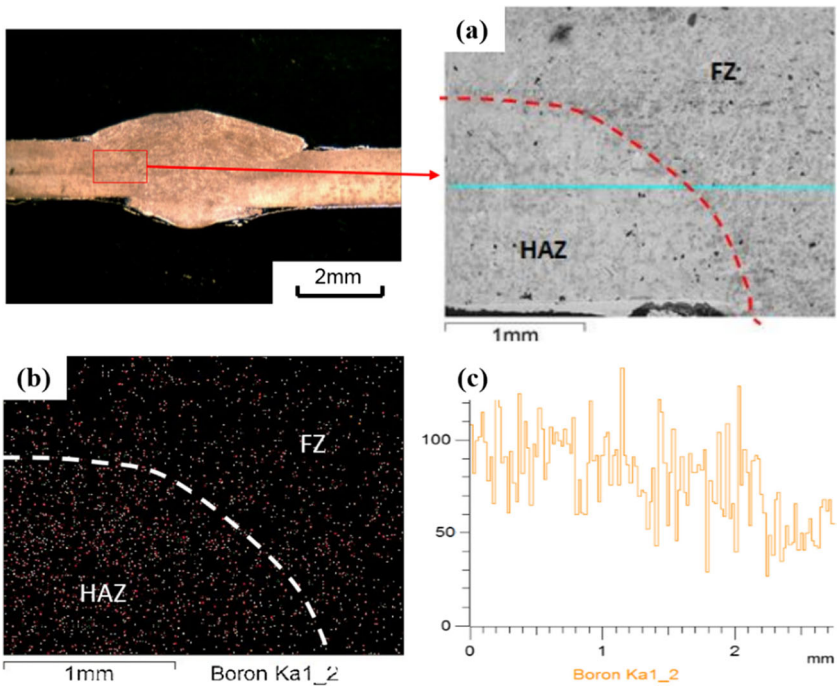

Fig. 8 EDX result for boron distribution at **a** HAZ–FZ boundaries by **b** area mapping and **c** line scanning of heat-treated specimen

HAZ. The dilution of welding filler without boron content and the parent metal in FZ produced lower hardness compared with that in HAZ. Base metal hardness remained the lowest and weakest at an average value of 187 HV, which might cause fractures in this area. For heat-treated specimen, the highest hardness value was also located at HAZ with 589 HV, followed by base metal and then FZ sequentially, as shown in Fig. 7b. The average hardness values of FZ and base metal were 513 and 391 HV, respectively. The hardness values of both areas were increased with the transformation of microstructure into martensite after heat treatment. However, the hardness values decreased to below 400 HV at the region between FZ and HAZ, which might be identified as a softened region.

This finding is supported by Hwang [15], who stated that heat during welding causes microstructure transformation. Theoretically, in heat treatment, solute boron segregates at austenite grain boundaries and retards the nucleation of pro-eutectoid ferrite. Nonetheless, the excessive boron atoms at this area facilitate the formation of borocarbide, $M_{23}(C,B)_6$, which acts as a nucleation site for ferrite, thereby producing the softened region. In addition, the difference in boron content at FZ and HAZ might promote the difference in hardness values. Mapping and line scanning on EDX analyses are conducted at HAZ and FZ boundaries, as shown in Fig. 8. Line scan results show the decrease in boron content in FZ (Fig. 8c). This result was clarified with the mapping analysis shown in Fig. 8b. Boron distribution was lesser in FZ than in HAZ. However, the existence of boron in FZ proved that boron is transferred from base metal. This phenomenon occurred with the dilution of parent metal and welding filler in

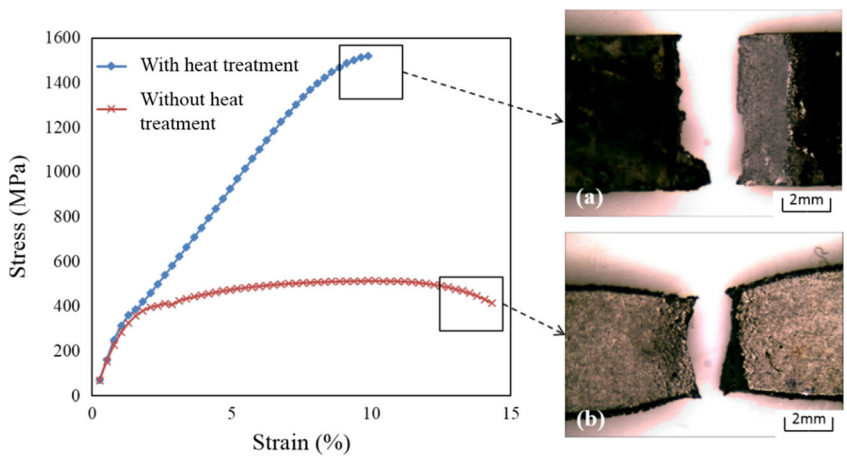

Fig. 9 Tensile strength and top view of fracture for **a** heat-treated specimen located at PMZ and **b** specimen without heat treatment located at base metal

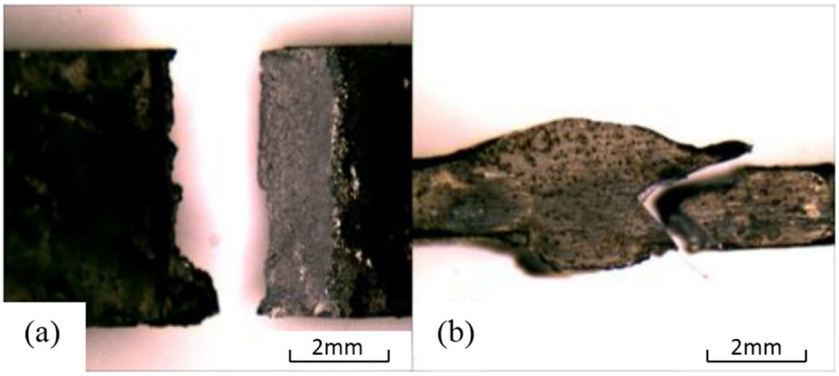

Fig. 10 Fracture location of heat-treated specimen at PMZ. **a** Top view. **b** Side view

molten metal flow during welding and caused the increased hardness in FZ after heat treatment.

3.3 Tensile test

Tensile test results of specimens with and without heat treatment and base metal specimens are shown in Fig. 9. The average UTS value is obtained from three samples of each specimen. The UTS value for the base metal sample is 504 MPa and that without heat treatment is approximately 500 MPa. Heat-treated specimen showed a high UTS value ranging between 1300 and 1400 MPa. This value is almost twofold higher than that of base metal. The fracture of the specimen without heat treatment is located at base metal area, thereby resulting in a strength value similar to that of base metal specimen. This result also indicated that strength is higher in welded area than in base metal. Fracture can be categorized as ductile because elongation reached 15% of the actual length and produced a width reduction at the fracture region, as shown in Fig. 9b.

As shown in Fig. 10, the fracture of heat-treated specimen is occurred at partially melted zone (PMZ) region. This fracture exhibited no width reduction and less elongation compared with that of the specimen without heat treatment. Fracture propagation might be due to the softened region discussed in hardness test results. Hence, the fracture in heat-treated specimen is observed to discuss the cause of fracture behavior at the softened zone.

3.4 Fracture analysis

Fracture on the heat-treated specimen is analyzed. As shown in Fig. 11, the fracture surface located at the PMZ region, which presented the lowest hardness value, shows a small irregular shallow dimple. The dimple indicated the intergranular fracture of grain structure that started from the grain boundary during fracture. The microvoids were identified as precipitates along the grain boundaries. The observed dimple also considerably reduced the bonding between the particles and the matrix, thereby decreasing fracture energy. This energy reduction promoted rapid crack propagation along grain boundaries. A few researchers also studied the precipitation along austenite grain boundaries.

Devletian [24] and Kapadia [25] studied boron steel welding and found that borocarbide precipitation at prior austenite grain boundaries can significantly decrease hardenability and notched toughness. They also observed that the soluble or uncombined boron during welding is responsible for borocarbide, $M_{23}(C,B)_6$, formation in HAZ. This formation depends on welding cooling rate and peak temperature, in which a high peak temperature during welding in HAZ near the FZ results in high tendency to form borocarbide upon cooling. This observation is supported by the latest study of

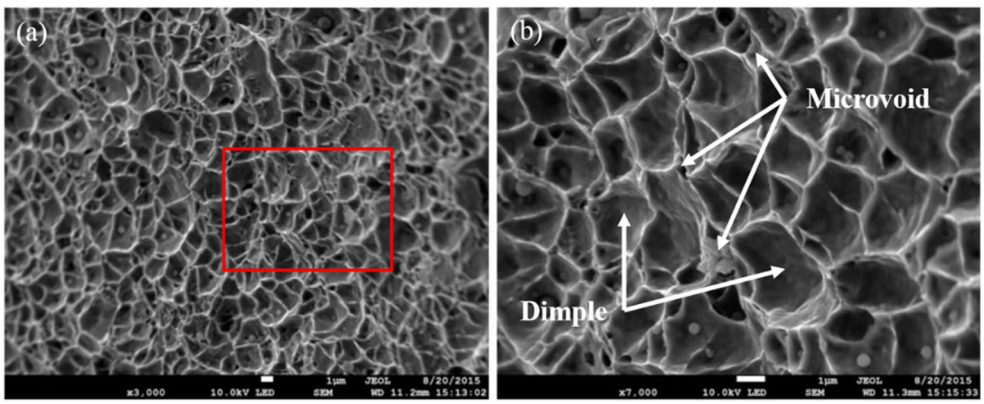

Fig. 11 Fracture surface of heat-treated specimen under SEM with **a** × 3.0 k magnification and **b** × 7.0 k magnification shows dimple and microvoid coalescence existence

Suski and Oliveira in 2013 [26]; they stated that a maximum limit exists in boron segregation-induced formation of borocarbides. Such limit also applies to borocarbide precipitation along austenite grain boundaries, which tend to promote ferrite nucleation events and thereby reduce hardness value. Also, Li et al. [27] reported that boron segregation at prior austenite grain boundaries during cooling was controlled by a non-equilibrium mechanism.

The relation in the present study is the fracture location of heat-treated specimen (PMZ or HAZ region near FZ). PMZ area experienced high heat input and cooling rate during welding. This location near FZ tended to attract the solute boron rally in this area. Non-control of peak temperature and cooling rate during welding resulted in the tendency of solute boron to precipitate borocarbide along the austenite grain boundary and promote ferrite nucleation. This condition also caused low hardness in this area. Furthermore, fracture topography showing dimples of microvoid likely proves the existence of borocarbide or another precipitation element and reduced the bonding between the grain and resulting intergranular fracture.

4 Conclusion

This study aimed to determine the effect of heat treatment on the microstructure and mechanical properties of boron steel welded using GMAW. The following conclusions can be drawn:

i. The specimen without heat treatment consisted of ferrite and pearlite at base metal, martensite at HAZ, and AF at FZ. The entire microstructure of heat-treated specimen was transformed into martensite.
ii. The boron from parent metal was transferred to the FZ via dilution of weld metal during welding, and its properties were enhanced after heat treatment.
iii. Intergranular fracture resulted at softened region of PMZ likely caused by borocarbide precipitation in austenite grain boundaries which promote ferrite nucleation.

Acknowledgements The authors would like to thank the supervisors and technical staff in Universiti Malaysia Pahang, where all of the experimental works were conducted. We also acknowledge the financial support from the Ministry of Education Malaysia (Research Grant Project No. RDU130112) through the Universiti Malaysia Pahang.

References

1. Tamarelli CM (2011) AHSS 101: the Evolving Advanced High-Strength steel for automotive applications. Steel Market Development Institute Report, Southfield, MI, USA
2. Xiaodong Z, Zhaohui M and Li W (2007) Current status of advanced high strength steel for auto-making and its development in Baosteel. Baosteel Res Inst, Shanghai, 201900:1–8
3. Gan W, Babu SS, Kapustka N, Wagoner RH (2006) Microstructural effects on the springback of advanced high-strength steel. Metall Mater Trans A 37:3221–3231
4. Chen G, Shi MF, Tyan T (2012) Optimized AHSS structures for vehicle side impact *SAE Int*. J Mater Manuf 5:304–313
5. Chen G, Shi MF, Tyan T (2011) Fracture modeling of AHSS in component crush tests *SAE*. Int J Mater Manuf 4:1–9
6. Chen G (2010) Optimized design solutions for roof strength using advanced high strength steels. SAE Int J Mater Manuf 3:90–98
7. Uchihara M (2011) Joining technologies for automotive steel sheets. Weld Int 25:249–259
8. Karbasian H, Tekkaya AE (2010) A review on hot stamping. J Mater Process Technol 210:2103–2118
9. Devletian JH, Heine RW (1975) Effect of boron content on carbon steel welds. Weld J *(Miami, Fla)* 54:45–53
10. Naderi M, Ketabchi M, Abbasi M, Bleck W (2011) Analysis of microstructure and mechanical properties of different boron and non-boron alloyed steels after being hot stamped. Procedia Eng 10:460–465
11. Turetta A, Bruschi S, Ghiotti A (2006) Investigation of 22MnB5 formability in hot stamping operations. J Mater Process Technol 177:396–400
12. Guerra LFV, Bedolla-Jacuinde A, Mejia I, Zuno J, Maldonado C (2015) Effects of boron addition and austempering time on microstructure, hardness and tensile properties of ductile irons. Mater Sci Eng A 648:193–201
13. Järvinen H, Isakov M, Nyyssönen T, Järvenpää M, Peura P (2016) The effect of initial microstructure on the final properties of press hardened 22MnB5 steels. Mater Sci Eng A 676:109–120
14. Naderi M (2007) *Hot stamping of ultra high strength steels* (RWTH Aachen University)
15. Hwang B, Suh D-W, Kim S-J (2011) Austenitizing temperature and hardenability of low-carbon boron steels. Scr Mater 64:1118–1120
16. Kim S, Kang Y, Lee C (2013) Variation in microstructures and mechanical properties in the coarse-grained heat-affected zone of low-alloy steel with boron content. Mater Sci Eng A 559:178–186
17. Bonnen JJF, Mandapati R, Kang H, Iyengar RM, Khosrovaneh AK, Amaya MA, Citrin K, Shih H-C (2009) Durability of advanced high strength steel gas metal arc welds. SAE Int J Mater Manuf 2:155–171
18. Suh CH, Lee RG, Oh SK, Jung Y, Son J, Kim YS (2011) Effect of welding heat input on fatigue life of quenched boron steel and FB steel lap joint. J Mech Sci Technol 25:1727–1735
19. Jong Y-S, Lee Y-K, Kim D-C, Kang M-J, Hwang I-S, Lee W-B (2011) Microstructural evolution and mechanical properties of resistance spot welded ultra high strength steel containing boron. Mater Trans 52:1330–1333
20. Lin H, Ying L, Jun L, Binghong L (2014) Microstructure and mechanical properties for TIG welding joint of high boron Fe-Ti-B alloy. Rare Met Mater Eng 43:283–286
21. Rafiqul M I, Ishak M and Rahman M M (2012) Effects of heat input on mechanical properties of metal inert gas welded 1.6 mm thick galvanized steel sheet, IOP Conf Ser Mater Sci Eng **36**
22. Li F, Fu M, Lin J (2014) Effect of cooling path on phase transformation of boron steel. Procedia Eng 81:1707–1712
23. Larn RH, Yang JR (2000) The effect of compressive deformation of austenite on the bainitic ferrite transformation in Fe Mn Si C steels. Mater Sci Eng A 278:278–291
24. Devletian J (1976) Borocarbide precipitation in the HAZ of boron steel welds. Weld Res Suppl 5–12
25. Kapadia BM (1987) Effect of boron additions on the toughness of heat-treated low-alloy steels. J Heat Treat 5:41–53
26. Suski CA, Oliveira CAS (2013) Effect of austenitization temperature on the precipitation of carbides in quenched low carbon boron steel. Metallogr Microstruct Anal 2:79–87
27. Li YJ, Ponge D, Choi P, Raabe D (2015) Segregation of boron at prior austenite grain boundaries in a quenched martensitic steel studied by atom probe tomography *Scr*. Mater 96:13–16